Geophysical Research Letters

RESEARCH LETTER
10.1029/2019GL085031

Convective Precipitation Efficiency Observed in the Tropics

Sugata Narsey[1,2,3], Christian Jakob[1,2], Martin S. Singh[1], Martin Bergemann[1,4], Valentin Louf[1], Alain Protat[3], and Christopher Williams[5]

[1]School of Earth, Atmosphere and Environment, Monash University, Clayton, Victoria, Australia, [2]Australian Research Council Centre of Excellence for Climate Extremes, Sydney, New South Wales, Australia, [3]Australian Bureau of Meteorology, Melbourne, Victoria, Australia, [4]Max Planck Institute for Meteorology, Hamburg, Germany, [5]Colorado Center for Astrodynamics Research (CCAR), University of Colorado Boulder, Boulder, CO, USA

Key Points:
- First long-term observational estimate of precipitation efficiency at convective scales for a location in the tropics is presented
- Precipitation efficiency increases with environmental humidity and decreases weakly with instability (CAPE)
- Compensation between precipitation efficiency and updraft velocity results in weak dependence of precipitation intensity on synoptic regime

Correspondence to:
S. Narsey,
sugata.narsey@bom.gov.au

Citation:
Narsey, S., Jakob, C. N., Singh, M. S., Bergemann, M., Louf, V., Protat, A., & Williams, C. (2019). Convective precipitation efficiency observed in the tropics. *Geophysical Research Letters*, *46*. https://doi.org/10.1029/2019GL085031

Received 16 AUG 2019
Accepted 18 NOV 2019
Accepted article online 26 NOV 2019

Abstract Precipitation efficiency refers to the fraction of condensate in the atmosphere that reaches the surface as precipitation. A high-quality data set of radar-estimated precipitation rates and convective scale vertical velocity near Darwin, Australia, is used to construct the first estimate of precipitation efficiency at convective scales for a long record of observations in the tropics. It is found that precipitation efficiency increases with precipitation rate and midtropospheric humidity and decreases with increasing convective available potential energy and surface temperature. Precipitation efficiency is largest under moist monsoonal conditions and smallest during monsoon break periods, which are characterized by a drier free troposphere. However, these differences in efficiency do not translate to differences in the instantaneous precipitation rate across the synoptic regimes because of a compensating change in the net condensation rate. This is driven by variations in cloud updraft velocity, which is larger in drier environments than in moist environments.

1. Introduction

While precipitation extremes are projected to increase under global warming (O'Gorman, 2015), less is known about precipitation extremes at convective scales. A useful approach is to decompose changes in precipitation extremes into thermodynamic, dynamic, and microphysical components (e.g., Muller et al., 2011; O'Gorman & Schneider, 2009). At large scales, projected changes in precipitation extremes are known to depend on the thermodynamic component through changes in humidity and the dynamic component through changes in the circulation (Chadwick et al., 2012; Pfahl et al., 2017). However, recent idealized modeling studies have shown that at convective scales, precipitation extremes may also be sensitive to microphysical processes that influence precipitation efficiency (Bao & Sherwood, 2018; Singh & O'Gorman, 2014).

To our knowledge there are no long record observation-based estimates of precipitation efficiency at convective scales, and very little observational evidence of how precipitation efficiency might be modulated by the large-scale environment. Here, we use a suite of recently produced observation-based data sets of precipitation and other variables at convective scales in the tropical north of Australia to produce the first such long-term estimate of precipitation efficiency.

Precipitation efficiency is usually defined as the ratio of precipitation to either the total condensation (microphysical efficiency) or the sum of moisture convergence and surface evaporation (large-scale efficiency). Sui et al. (2007) provide a summary of these definitions and show them to be highly correlated. Observation-based studies tend to focus on a large-scale efficiency (e.g., Chong & Hauser, 1989) as the terms in the definition are more readily estimated from observations such as soundings and flux measurements. While there have been some studies attempting to estimate precipitation efficiency at storm scales (e.g., Braham, 1952; Market et al., 2003; Newton, 1966), these are based on small numbers of events and are located outside of the tropics. Some studies have attempted to estimate precipitation efficiency using observations for single events in the tropics (e.g., Chong & Hauser, 1989; Oury et al., 2000), but such analyses cannot be used to infer relationships between precipitation efficiency and the large-scale state of the atmosphere. Bailey et al. (2015) estimate precipitation efficiency for a location in the subtropics, although their results are obtained indirectly through the use of water vapor isotope measurements. Lau and Wu (2003) estimate

precipitation efficiency using satellite-based data; however, their calculations rely on threshold assumptions of conversion from cloud condensate to precipitation (i.e., a parameterization).

In the present study we adopt a definition of precipitation efficiency used in previous studies of convective precipitation extremes (Muller & Held, 2012; Muller et al., 2011; Singh & O'Gorman, 2014). This definition differs somewhat from more traditional definitions (e.g., Sui et al., 2007) in that it is based on the dry static energy budget, rather than a budget for water vapor or a budget for precipitating hydrometeors. Furthermore, we follow Muller et al. (2011) in defining precipitation efficiency using the net condensation within the column (condensation minus evaporation) rather than the total condensation. We focus solely on precipitation efficiency at convective scales. There will likely be some differences between precipitation efficiency at large scales and convective scales; however, these are not addressed here.

Idealized cloud resolving modeling studies of precipitation efficiency have found varying sensitivities of precipitation to surface temperature (Lutsko & Cronin, 2018; Muller et al., 2011; Singh & O'Gorman, 2014), convective organization (Bao & Sherwood, 2018; Muller & Held, 2012), and large-scale circulation (Lutsko & Cronin, 2018). Such studies imply that precipitation efficiency is strongly modulated by the large-scale state of the atmosphere, but at present, there is little observational evidence with which to verify this. This may largely be due to a lack of suitable observations needed to estimate precipitation efficiency at convective scales, where both the precipitation and net condensation vary rapidly.

To estimate precipitation efficiency, we employ a recently available long-period high-quality data set of dual-polarization radar-derived rainfall as well as dual-frequency wind profiler-derived vertical motion for a site in the tropics located near Darwin, Australia. These observations have provided a unique opportunity to observe the relationship between precipitating convection and vertical motion, particularly relevant to convective mass flux at climate model grid scales (Kumar et al., 2015, 2016). Likewise, understanding the factors influencing precipitation efficiency could be useful for improving predictions of extreme precipitation in a warmer climate.

The first goal of the present study is to provide the first ever observational estimates of precipitation efficiency using the Darwin observatory. A second, equally important goal, is to understand how efficiency might relate to the state of the atmosphere in which the precipitating systems are embedded.

2. Data and Methods

Following Muller et al. (2011), a simple approximate expression for precipitation is

$$P = -\epsilon \int_{sfc}^{ctop} w \frac{dq_{sat}}{dz} \rho \mathrm{d}z \quad , \tag{1}$$

where P is the precipitation, ϵ is the precipitation efficiency, w is the vertical velocity, z is the height coordinate, and q_{sat} is the saturation mixing ratio. The integral on the right-hand side of equation (1) is the net condensation and is evaluated between the surface and the cloud top height. The derivation for this equation is applicable on convective scales in the tropics, and it relies on the assumption of weak temperature gradients in the troposphere, valid in the tropics, in order to neglect horizontal advection and the Eulerian tendency of dry static energy. Furthermore, equation (1) assumes that the atmospheric stratification is close to moist adiabatic. This second assumption may be relaxed by replacing saturation mixing ratio q_{sat} in equation (1) with the dry static energy. We found this to not significantly change the results presented below although it did increase the magnitude of precipitation efficiency overall (not shown). A similar scaling derived based on parcel theory is given in O'Gorman and Schneider (2009).

The estimation of precipitation efficiency from equation (1) requires colocated estimates of surface precipitation and vertical profiles of vertical velocity and saturation specific humidity from the surface to the cloud top.

To estimate precipitation we use a relatively new data set of C-band polarimetric (CPOL) radar observations spanning the wet seasons (October to April) between 1998 and 2017 (Louf, Protat, et al., 2019). Precipitation is estimated using the dual-polarization relationships found by Thompson et al. (2018), specifically tuned for this location. The CPOL data set is provided on a 1-km grid every 10 min and constitutes one of the few long-term high-quality radar data sets in the tropics.

In our expression for precipitation efficiency (equation (1)) we integrate net condensation from the surface to the cloud top height. Following Jackson et al. (2018), we estimate cloud top height from the CPOL radar data set using the 0-dBz echo top height algorithm of Lakshmanan et al. (2013).

Vertical wind is retrieved for the period 1998 to 2012 using a pair of Doppler radar vertical wind profilers located at Darwin (Williams, 2012), approximately 12.4°S and 130.9°E. The two wind profilers have frequencies of 920 and 50 MHz, and from these it is possible to separate the contributions of vertical air velocity and the influence of hydrometeor fall speed, resulting in accurate estimates of updrafts and downdrafts (Williams, 2012). The pair of profilers is able to retrieve vertical wind at a temporal frequency of 1 min at levels spaced 100 m apart, from approximately 1,400 m above the ground. These near-instantaneous measurements are then averaged to 10-min intervals in time and 500-m intervals vertically in order to match the vertical resolution of the saturation mixing ratio profiles, described below. The lowest 1,400 m is infilled by assuming the vertical wind is constant at the 1,400-m value. Similar results are obtained if the vertical velocity is linearly interpolated from its value at 1,400 m to 0 at the surface.

The large-scale environmental vertical profile of saturation mixing ratio is obtained using a constrained variational analysis of sounding data within the CPOL radar domain encompassing a region with an approximate radius of 150 km (Xie et al., 2010; Zhang & Lin, 1997). In this approach initial estimates of the profiles are sought from the European Centre for Medium-Range Weather Forecasts analysis data and are adjusted based on observations, including rainfall from the CPOL data set. Here optimization constraints include the conservation of mass, moisture, heat, and momentum. For details on the application of this method in the Darwin region, see Davies et al. (2013). The variational analysis provides a best estimate of the large-scale environment for convective events within the CPOL radar domain. Estimates of the large-scale state from the variational analysis are given every 6 hr. While this temporal resolution is far coarser than other observations used in this study, we argue that this is a reasonable approximation since saturation mixing ratio is a thermodynamic function of temperature and pressure and therefore does not vary rapidly for the large-scale environment for most situations in the tropics.

To calculate precipitation efficiency using equation (1), the radar-estimated precipitation rate is colocated in time and space with vertical wind profiler measurements. The nearest (in time) environmental profile of saturation mixing ratio is also matched with each wind profiler sample. In order to focus on precipitation events for which our method can produce reasonable estimates of efficiency, some filtering is necessary. Only the convective rainfall events are selected by applying the Steiner et al. (1995) convective-stratiform classification to the CPOL data set. This is done to avoid stratiform rainfall, where the updrafts may be weak or dissociated in space and time from the pixel precipitation rate, and also because equation (1) only applies to strong local precipitation. Applying the additional criteria of an arbitrary precipitation rate threshold of 5 mm/hr did not change the key results presented in this study (not shown). A simple spatial and temporal moving average smoothing is applied to the precipitation data set to minimize the likelihood of missing the estimated instantaneous precipitation associated with a 10-min time-averaged updraft. The smoothing window is limited to 10 min on either side of each convective event and 1 km around the profiler site.

The above method gives a set of 1,122 collocated estimates of precipitation and net condensation rate over the 15 years of observations. In principle, a separate precipitation efficiency may be calculated for each event by taking the ratio of these estimates. However, the resultant precipitation efficiency is highly error prone due to the appearance of an uncertain estimate of net condensation in the denominator. Instead, we first aggregate the precipitation and net condensation over subsets of the available events based on, for example, the large-scale environmental conditions during the event. We then calculate the precipitation efficiency as the ratio of the mean precipitation rate to the mean net condensation rate over each subset. Calculating the precipitation efficiency for each event and taking the mean gave qualitatively similar results (not shown).

The subsets described above are defined based on large-scale environmental parameters such as the midtropospheric humidity, convective available potential energy (CAPE), or the synoptic regime. The large-scale environmental parameters are calculated using the variational analysis data and therefore represent estimates of the state of the atmosphere on scales large compared to individual convective events. Here, the CAPE is calculated as the vertical integral of the positive buoyancy of a surface parcel lifted to the top of the atmosphere. Here we assume reversible thermodynamics with ice as a fraction of condensate increasing linearly from 273.16 K (no ice) to 233.16 K (completely ice). This calculation is done using temperature and moisture from the variational analysis data set. Lag relationships between CAPE and precipitation are

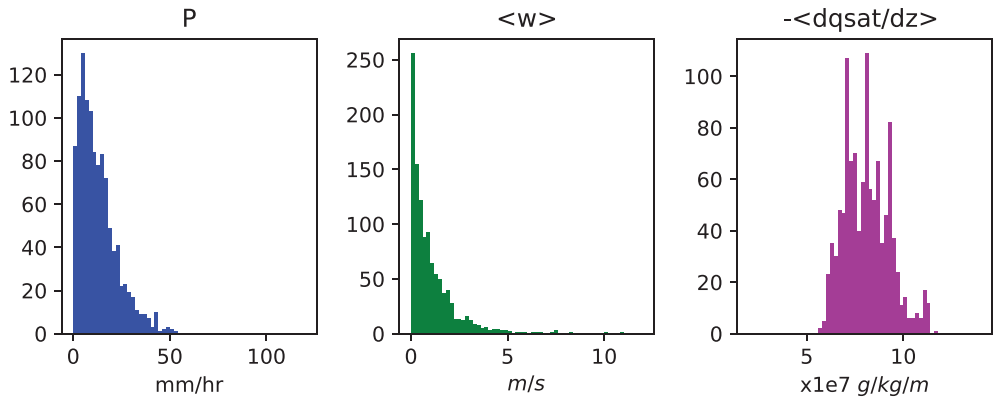

Figure 1. Histograms of precipitation P (blue), vertically integrated mass-weighted vertical motion <w> (green), and vertically integrated mass-weighted vertical gradient of saturation mixing ratio $<\frac{dq_{sat}}{dz}>$ (magenta).

known to occur in reality; however, in the present study we assert that the nearest-in-time 6-hourly estimate of CAPE calculated for the large-scale environment is the most relevant estimate for the convective events studied. While local conditions more relevant to parcel theory would be ideal for such calculations, suitable observations are simply not available for our study site.

In order to characterize the large-scale environment, we use the Darwin wet season synoptic regimes defined by Pope et al. (2009). These regimes are determined by clustering wind and thermodynamic profiles from radiosonde data near Darwin for 49 wet seasons. Three of these distinct regimes are prevalent in the northern Australian wet season, particularly during precipitation events. These are the deep westerly (DW) regime characteristic of monsoon bursts and the shallow westerly (SW) and moist easterly (ME) regimes characteristic of monsoon buildup or breaks.

3. Results

Histograms of precipitation (P), updraft strength (quantified as the vertically integrated mass-weighted vertical velocity, <w>), and thermodynamic state (quantified as the vertically integrated mass-weighted vertical gradient of saturation mixing ratio, $<\frac{dq_{sat}}{dz}>$) are shown in Figure 1. The P and <w> histograms are skewed toward lower values, while the $<\frac{dq_{sat}}{dz}>$ histogram is closer to symmetric about the mean. We note here that the histogram of $<\frac{dq_{sat}}{dz}>$ appears to be noisier than that for P and <w>. This is likely due to variations near the surface, with similar histograms found for surface temperature and pressure (not shown).

We now study the relationship between the terms in equation (1) as a function of the large-scale state of the atmosphere. First, we divide our data set according to terciles of precipitation rate (top row of Figure 2). The relationship between terciles of precipitation rate and updraft strength <w> is found to be statistically significant (p values < 0.05) using a Student's t test. The vertical gradient in saturation mixing ratio does not vary strongly with precipitation rate. Precipitation efficiency is estimated using the mean values of precipitation and net condensation for each tercile, and it is found to strongly increase with precipitation rate. The increase in both updraft strength <w> and precipitation efficiency with precipitation rate suggests that both variations in the dynamical and microphysical character of convective events contribute to their observed intensity. Sensitivity tests lagging precipitation and vertical velocity profiles show qualitatively similar results to those presented here. Peaks in both precipitation and vertical velocity at time lag 0 (not shown) increase our confidence in the relationships inferred from our results.

Next we investigate the components of equation (1) presented by terciles of CAPE, midtropospheric moisture, precipitable water, and surface temperature (Figure 2). These are estimated from the variational analysis and are representative of the large-scale state of the atmosphere. Precipitation rates decrease weakly with larger CAPE and increase with midtropospheric moisture, although for both we only find a statistically significant change between the first two terciles. Updraft strength does not vary strongly with CAPE (no statistical significance), although it decreases as midtropospheric moisture becomes larger (significant only between second and third terciles). The mean vertical gradient in saturation mixing ratio increases significantly with increased CAPE and decreases significantly with larger midtropospheric moisture. Precipitation

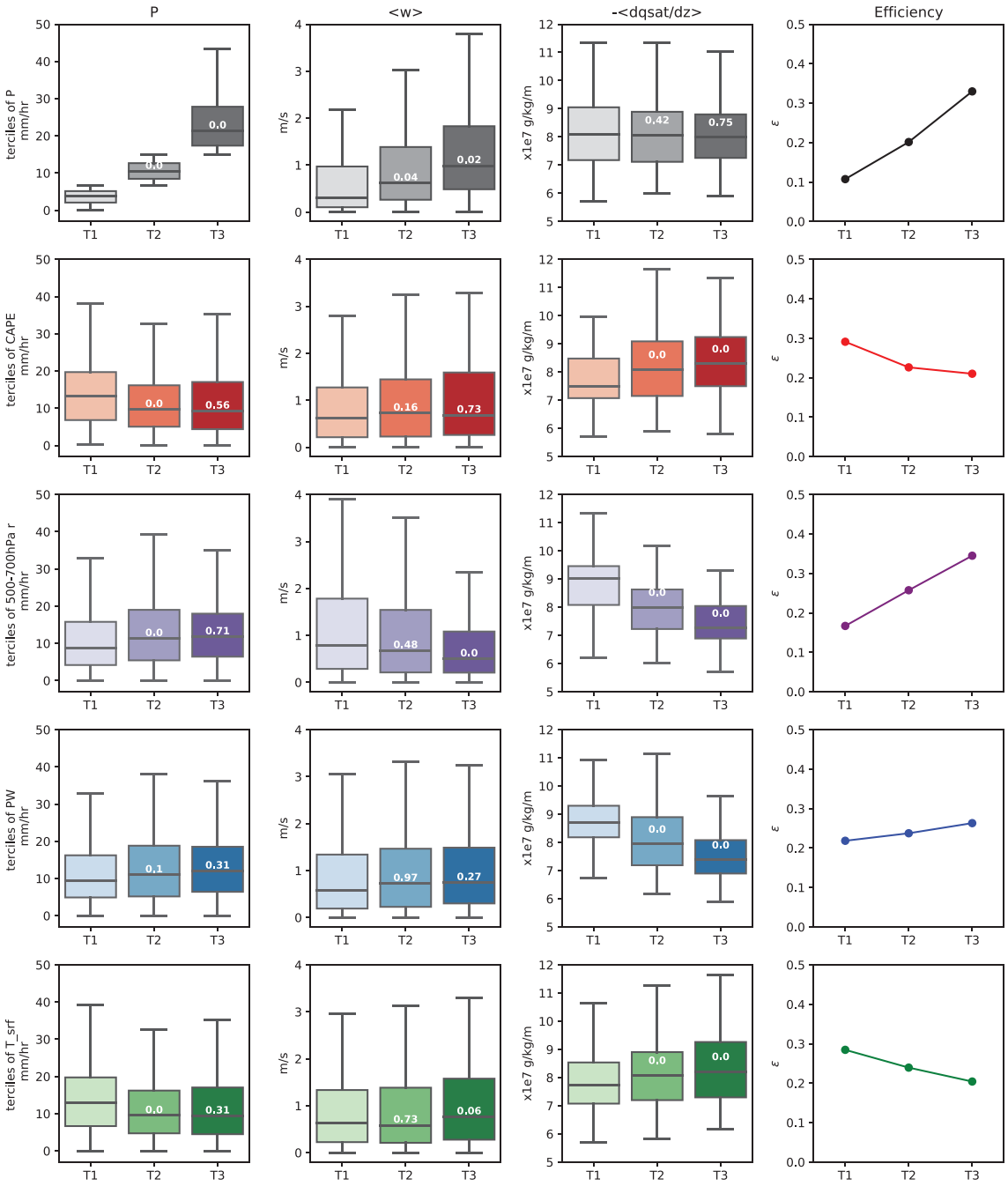

Figure 2. Boxplots of precipitation rate P, vertically integrated mass-weighted updraft $<w>$, vertically integrated mass-weighted vertical derivative of saturation mixing ratio $<\frac{dq_{sat}}{dz}>$, and line plots of precipitation efficiency ϵ, according to terciles of precipitation rate (top row—gray shading), CAPE (second row—red shading), 500- to 700-hPa mean mixing ratio (third row—purple shading), precipitable water (fourth row—blue shading), and surface temperature (bottom row—green shading). Efficiency is calculated using the mean precipitation rate and mean condensation rate for each tercile. The statistical significance of each tercile sample mean is quantified using a two-sided Student's t test, by comparing each tercile against the adjacent lower tercile. The p value is displayed over each boxplot, with the differences being significant where the p value is below 0.05.

efficiency decreases weakly with larger CAPE but increases strongly with midtropospheric moisture. Precipitable water showed similar relationships to those for midtropospheric moisture, although slightly weaker (fourth row of Figure 2). Precipitation and updraft velocity are not found to vary strongly with surface temperature (bottom row of Figure 2); however, significant differences in $<\frac{dq_{sat}}{dz}>$ are found between terciles of surface temperature. This results in an inverse relationship between surface temperature and precipitation

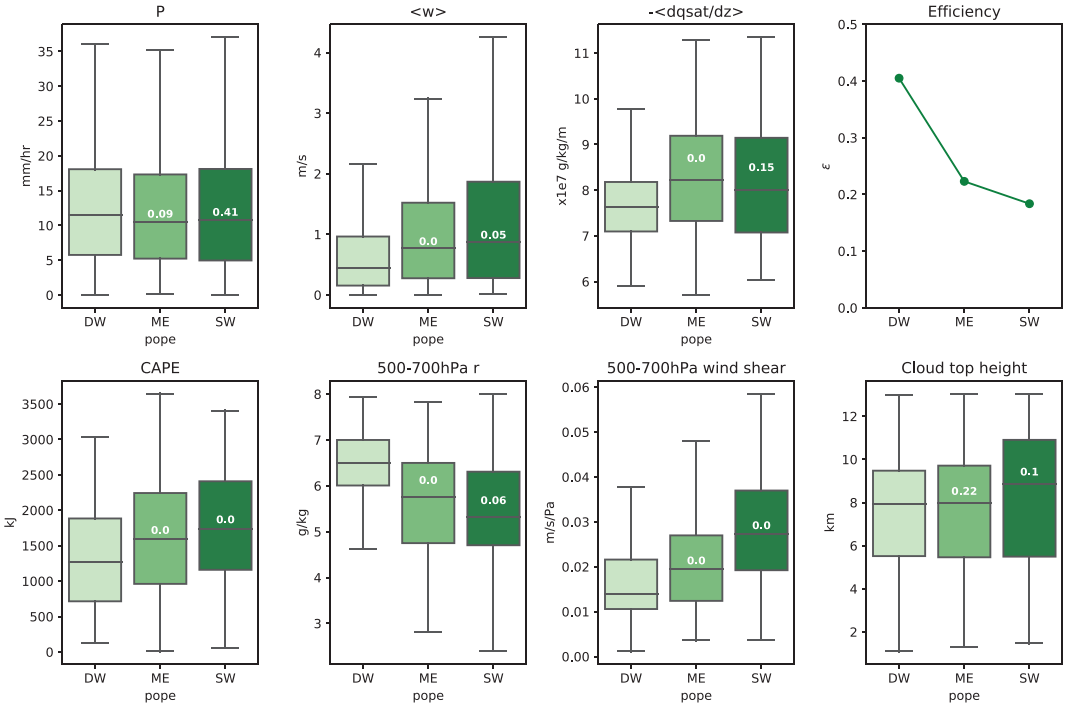

Figure 3. Boxplots of several variables according to Darwin wet season synoptic regimes, labeled in order, deep westerly (DW), moist easterly (ME), and shallow westerly (SW) regimes. For the top row in order, precipitation rate P, vertically integrated mass-weighted updraft $<w>$, vertically integrated mass-weighted vertical derivative of saturation mixing ratio $<\frac{dq_{sat}}{dz}>$, and line plots of precipitation efficiency ϵ. Efficiency is calculated using the mean precipitation rate and mean condensation rate for each regime. For the bottom row in order, total convective available potential energy (CAPE), mixing ratio averaged between 500 and 700 hPa, vertical wind shear averaged between 500 and 700 hPa, and cloud top height. The statistical significance of each regime sample mean is quantified using a two-sided Student's t test, by comparing each sample against the left-adjacent box sample. The p value is displayed over each boxplot, with the differences being significant where the p value is below 0.05.

efficiency. Overall, these large-scale conditions appear to partially modulate precipitation efficiency and its influencing components.

An interesting question is how precipitation efficiency and its contributing components are related to the large-scale dynamical state of the atmosphere in which the convective systems are embedded. Pope et al. (2009) have classified the large-scale atmospheric states associated with the wet season over Darwin using a small number of synoptically distinct regimes, three of which are associated with rainfall. Respectively, these are a DW regime associated with active monsoon conditions and a moist easterly (ME) and SW regime, which are both associated with monsoon break conditions. The DW regime is characterized by a deep layer of westerly winds over Darwin extending from the surface to just above 400 hPa, and high precipitable water (40 to 60 mm). The synoptic pattern for the DW regime is typical of the active monsoon with a broad trough over the north of Australia and widespread precipitation. The ME regime is characterized by a layer of easterly winds near the surface and westerly winds aloft, with high precipitable water (40 to 55 mm). The synoptic pattern for the ME regime is typical of monsoon breaks, with suppressed conditions over northern Australia and easterly trade winds extending from the Coral Sea toward the west of the continent. The SW regime is characterized by a shallow layer of westerly winds (below 800 hPa) with easterlies aloft and lower precipitable water (35 to 50 mm). The synoptic pattern associated with the SW regime has lower pressure over the eastern part of the continent, with westerly winds extending into the Coral Sea, consistent with a transition from active to break conditions.

The components of equation (1) are stratified according to synoptic regimes, presented in Figure 3. Surprisingly, the instantaneous local precipitation rate (10-min 1-km grid spacing) is almost invariant with the synoptic regime. This seemingly contradicts many past studies (e.g., Pope et al., 2009), which have shown that convection in Darwin is much more vigorous during the break periods and less strong during the

monsoon. However, this apparent contradiction can be resolved when assessing the distributions of efficiency and vertical motion according to synoptic regime. Efficiency is larger for the DW regime than for the moist easterly and SW regimes. However, the mean updraft strength $<w>$ is weakest for the DW regime and stronger for the two regimes associated with monsoon break conditions (statistically significant between DW and ME categories and marginally significant between ME and SW). Similarly, $<\frac{dq_{sat}}{dz}>$ is lower for the DW regime (statistically significant between DW and ME categories). So the synoptic regimes appear to modulate the net condensation, although the influences of the efficiency and net condensation variations are compensating on average, with the net result being a similar spread in instantaneous precipitation rates in each regime.

A selection of environmental conditions associated with each synoptic regime is shown in the bottom row of Figure 3. The monsoon break environments (ME and SW) tend to have higher CAPE (statistically significant) and lower midtropospheric moisture (statistically significant) than the active monsoon regime (DW). The monsoon break regimes also have higher midtropospheric wind shear when compared to the DW regime (statistically significant). The relationship between cloud top heights and synoptic regimes is weak.

4. Discussion and Conclusions

We have presented the first long-term observational estimate of precipitation efficiency, based on equation (1) for convective precipitation in the tropics. Note that our definition of precipitation efficiency is affected by hydrometeor divergence from the column, consistent with Muller et al. (2011). While we attempt to isolate the influences of large-scale environmental conditions on precipitation efficiency, we acknowledge that in reality several of these conditions may covary. For example, synoptic regimes may modulate profiles of temperature and moisture, making it difficult to fully separate their influences.

We find that precipitation efficiency is not constant and in fact varies with precipitation rate and the large-scale state of the atmosphere (Figures 2 and 3). Higher precipitation rates are associated with higher net condensation (and updraft strength) as well as higher efficiency. CAPE is not found to be strongly related to precipitation rates, but larger CAPE is associated with lower efficiency. CAPE provides an upper limit to vertical motion, so it is perhaps unsurprising that the precipitation efficiency and CAPE are related. However, here we find that the updraft velocity is only weakly related to CAPE, and instead, it is the vertical profile of saturation mixing ratio that is most strongly related CAPE.

As expected from basic theory, precipitation efficiency increases with midtropospheric moisture. Similar relationships were found for lower and upper tropospheric moisture (not shown). However, due to a counterveiling decrease in the net condensation rate, the precipitation rate is relatively insensitive to the environmental humidity. We emphasize that the precipitation rate being measured here is at the convective scale, and so these results do not contradict previous studies that have highlighted the tight relationship between environmental humidity and the large-scale precipitation rate (e.g., Bretherton et al., 2004; Neelin et al., 2009).

Surface temperature is found to be inversely proportional to precipitation efficiency, with much of this relationship determined by differences in $<\frac{dq_{sat}}{dz}>$. While surface temperature may modulate precipitation rates through changes in atmospheric moisture or changes in convection (e.g., Dong et al., 2019; Lepore et al., 2015), we present here a third possibility: through changes to precipitation efficiency. However, it is likely that the observed relationship between efficiency and surface temperature is modulated by other covarying factors including relative humidity, limiting the direct applicability of this finding to a changing climate. Idealized modeling studies in fact suggest that precipitation efficiency will either remain the same (Muller et al., 2011) or potentially increase (Lutsko & Cronin, 2018; Singh & O'Gorman, 2014) with surface warming.

We also investigated the relationship between precipitation efficiency and the large-scale dynamical state of the atmosphere using a synoptic regime classification relevant to the northern Australian wet season (Pope et al., 2009). We find that precipitation efficiency (but not instantaneous local precipitation rate) varies with synoptic regime. During active monsoon conditions the precipitation efficiency is larger, updrafts are weaker, and the environment is moister. During monsoon break conditions precipitation efficiency tends to be lower, updrafts are stronger, and the environment is drier and has higher CAPE and wind shear. Stronger updrafts in this region are known to be associated with drier environments (Kumar et al., 2015, 2016; Protat & Williams, 2011). Our results are consistent with the observation-based estimates of efficiency conducted

by Bailey et al. (2015), with higher efficiency over Hawaii associated with moist plumes from the tropics. Similarly, our findings are consistent with those of Lutsko and Cronin (2018), who found that higher efficiency occurs in the ascending regions in their idealized model. Our results show that in regions of widespread ascent (active monsoon) the precipitation efficiency tends to be higher.

That the instantaneous precipitation rate of convective events is not modulated strongly by synoptic regimes is initially surprising, given that greater precipitation totals are associated with active monsoon compared to breaks (e.g., Nguyen et al., 2015; Protat et al., 2014). However, for northern Australia the area-averaged precipitation totals relate much more strongly to the convective area fraction than the convective intensity (Davies et al., 2013; Louf, Jakob, et al., 2019). In the present study we only consider instantaneous precipitation rates for convective events, which may be similar in intensity between regimes but differ in other ways, which we do not consider here such as frequency and duration of rain. How can we explain the differences in updraft strength yet indistinguishable observed precipitation rates between these regimes? We found that variations in precipitation efficiency had a compensating influence.

Does the degree of convection aggregation help explain the observed differences in precipitation efficiency (and the lack of difference in precipitation rates) between synoptic regimes? Using an idealized model, Bao and Sherwood (2018) found that convective self-aggregation leads to weaker updrafts, a warmer and moister local midtroposphere, and ultimately a higher precipitation efficiency, resulting in instantaneous precipitation extremes similar to that from disaggregated states. Although our active monsoon regime observations are not necessarily analogous to the self-aggregated states in their model, broadly speaking, they share some local environmental characteristics, for example larger midtropospheric moisture around the storm. The insensitivity of instantaneous precipitation rate to convective aggregation or organization is further supported by observational evidence showing that the local intensity of scattered convection is similar to that of organized convection (Tan & Oreopoulos, 2019).

Spatial smearing of rainfall as the result of turbulent motions on multiple scales (Singh & O'Gorman, 2014) may also influence the differences in precipitation efficiency between synoptic regimes. Vertical wind shear is smaller in the active monsoon environment than for the drier environments and seems consistent with the larger precipitation efficiency found for active monsoon conditions. However, one might expect greater spatial smearing due to cloud scale circulations in the active monsoon, where some of the convective cloud condensate eventually contributes to stratiform rain.

Reevaporation or sublimation of precipitation could also contribute to differences in precipitation efficiency between synoptic regimes. A drier environment will result in greater reevaporation of falling rain, and with all else being equal we would then expect lower precipitation efficiency, as we do observe. However, as noted previously this does not translate into differences in precipitation rates due to a counterbalancing change in net condensation. Why does this occur?

We find that the higher net condensation rates in the regimes characterized by drier environments are driven primarily by stronger updrafts, and they are associated with larger values of CAPE. Increased CAPE in drier environments was also found in the observational study of Singh et al. (2017), and they attributed this to the effect of convective entrainment on the tropospheric lapse rate (Seeley & Romps, 2015; Singh & O'Gorman, 2013). Alternatively, updraft strength may also be influenced by factors independent of CAPE; for example, a drier atmosphere may prevent weaker updrafts from growing to the upper troposphere, increasing the mean updraft strength through a process analagous to natural selection (Derbyshire et al., 2011).

Our results point to a substantial cancelation between variations in net condensation and efficiency with synoptic regime as well as with variations in the large-scale thermodynamic environment. Under a future warming scenario, the saturation deficit of the free troposphere is expected to increase following the Clausius Clapeyron relation. This increased saturation deficit has been argued to lead to increases in updraft velocity (Singh & O'Gorman, 2015) and may also be expected to affect precipitation efficiency through reevaporation (Lutsko & Cronin, 2018). This work provides a first step in providing an observational basis toward constraining how such dynamical and microphysical influences may affect future precipitation and its extremes.

We note some important caveats for the results presented here, primarily related to the limitations of our observation-based data. We selected convective events only; however, the overall efficiency may be influenced by stratiform rainfall events. We assumed that updrafts and precipitation are colocated in space and

time, which may not necessarily be true particularly for large convectively organized events. While we attempt to address this concern by calculating efficiency for subsets rather than for each event, systematic differences in convective organization or shear across different subsets may bias our estimates of the relationships between efficiency and the large-scale atmospheric state. Finally, methodological choices such as the moist adiabatic assumption and the resampling of observational data influence the magnitude of precipitation efficiency, although the relationships with the large-scale environment were more robust.

While we have attempted to decrease the error in our estimates of precipitation efficiency due to observational uncertainty, we acknowledge some uncertainty remains. Consequently, we cannot rule out that some real relationships may exist where we have found none. Despite these caveats, we are confident that our conclusions are qualitatively robust, since they withstood several sensitivity tests. Hence, we consider the present study to be a useful starting point for future research into convective precipitation efficiency in the tropics.

Future studies might consider how precipitation efficiency at convective scales relates to entrainment rate and other factors such as organization or aggregation, which are likely to modulate many of the large-scale characteristics of the atmosphere. Although the influence of convective organization is absent from most if not all convection parameterisations, simple observed relationships between large-scale environmental conditions and precipitation efficiency may help avoid introducing unnecessary complexity to climate models.

Acknowledgments
This research was supported by the Australian Research Council Centre of Excellence for Climate Extremes (CE170100023). Code to calculate thermodynamic quantities is publicly available at the website (https://gitlab.com/martinsingh/matlab_packages.git). The radar and large-scale data sets used in this study are available in the Atmospheric Radiation Measurement program archive (https://www.arm.gov/).

References

Bailey, A., Nusbaumer, J., & Noone, D. (2015). Precipitation efficiency derived from isotope ratios in water vapor distinguishes dynamical and microphysical influences on subtropical atmospheric constituents. *Journal of Geophysical Research: Atmospheres*, *120*, 9119–9137. https://doi.org/10.1002/2015JD023403

Bao, J., & Sherwood, S. C. (2018). The role of convective self-aggregation in extreme instantaneous vs. daily precipitation. *Journal of Advances in Modeling Earth Systems*, *11*, 19–33. https://doi.org/10.1029/2018MS001503

Braham, R. R. (1952). The water and energy budgets of the thunderstorm and their relation to thunderstorm development. *Journal of Meteorology*, *9*(4), 227–242. https://doi.org/10.1175/1520-0469(1952)009<0227:TWAEBO>2.0.CO;2

Bretherton, C. S., Peters, M. E., & Back, L. E. (2004). Relationships between water vapor path and precipitation over the tropical oceans. *Journal of Climate*, *17*(7), 1517–1528. https://doi.org/10.1175/1520-0442(2004)017<1517:RBWVPA>2.0.CO;2

Chadwick, R., Boutle, I., & Martin, G. (2012). Spatial patterns of precipitation change in CMIP5: Why the rich do not get richer in the tropics. *Journal of Climate*, *26*(11), 3803–3822. https://doi.org/10.1175/JCLI-D-12-00543.1

Chong, M., & Hauser, D. (1989). A tropical squall line observed during the COPT 81 experiment in West Africa. Part II: Water budget. *Monthly weather review*, *117*(4), 728–744.

Davies, L., Jakob, C., May, P., Kumar, V. V., & Xie, S. (2013). Relationships between the large-scale atmosphere and the small-scale convective state for Darwin, Australia. *Journal of Geophysical Research: Atmospheres*, *118*, 11,534–11,545. https://doi.org/10.1002/jgrd.50645

Derbyshire, S. H., Maidens, A. V., Milton, S. F., Stratton, R. A., & Willett, M. R. (2011). Adaptive detrainment in a convective parametrization. *Quarterly Journal of the Royal Meteorological Society*, *137*(660), 1856–1871.

Dong, W., Lin, Y., Wright, J. S., Xie, Y., Yin, X., & Guo, J. (2019). Precipitable water and CAPE dependence of rainfall intensities in China. *Climate Dynamics*, *52*(5-6), 3357–3368. https://doi.org/10.1007/s00382-018-4327-8

Jackson, R. C., Collis, S. M., Louf, V., Protat, A., & Majewski, L. (2018). A 17 year climatology of the macrophysical properties of convection in darwin. *Atmospheric Chemistry and Physics*, *18*(23), 17,687–17,704. https://doi.org/10.5194/acp-18-17687-2018

Kumar, V. V., Jakob, C., Protat, A., Williams, C. R., & May, P. T. (2015). Mass-flux characteristics of tropical cumulus clouds from wind profiler observations at Darwin, Australia. *Journal of the Atmospheric Sciences*, *72*(5), 1837–1855. https://doi.org/10.1175/JAS-D-14-0259.1

Kumar, V. V., Protat, A., Jakob, C., Williams, C. R., Rauniyar, S., Stephens, G. L., & May, P. T. (2016). The estimation of convective mass flux from radar reflectivities. *Journal of Applied Meteorology and Climatology*, *55*(5), 1239–1257. https://doi.org/10.1175/JAMC-D-15-0193.1

Lakshmanan, V., Hondl, K., Potvin, C. K., & Preignitz, D. (2013). An improved method for estimating radar echo-top height. *Weather and Forecasting*, *28*(2), 481–488.

Lau, K. M., & Wu, H. T. (2003). Warm rain processes over tropical oceans and climate implications. *Geophysical Research Letters*, *30*(24), 2290. https://doi.org/10.1029/2003GL018567

Lepore, C., Veneziano, D., & Molini, A. (2015). Temperature and CAPE dependence of rainfall extremes in the eastern United States. *Geophysical Research Letters*, *42*, 74–83. https://doi.org/10.1002/2014GL062247

Louf, V., Jakob, C., Protat, A., Bergemann, M., & Narsey, S. (2019). The relationship of cloud number and size with their large-scale environment in deep tropical convection. *Geophysical Research Letters*, *46*, 9203–9212. https://doi.org/10.1029/2019GL083964

Louf, V., Protat, A., Warren, R. A., Collis, S. M., Wolff, D. B., Raunyiar, S., et al. (2019). An integrated approach to weather radar calibration and monitoring using ground clutter and satellite comparisons. *Journal of Atmospheric and Oceanic Technology*, *36*(1), 17–39. https://doi.org/10.1175/JTECH-D-18-0007.1

Lutsko, N. J., & Cronin, T. W. (2018). Increase in precipitation efficiency with surface warming in radiative-convective equilibrium. *Journal of Advances in Modeling Earth Systems*, *10*, 2992–3010. https://doi.org/10.1029/2018MS001482

Market, P., Allen, S., Scofield, R., Kuligowski, R., & Gruber, A. (2003). Precipitation efficiency of warm-season midwestern mesoscale convective systems. *Weather and Forecasting*, *18*(6), 1273–1285. https://doi.org/10.1175/1520-0434(2003)018<1273:PEOWMM>2.0.CO;2

Muller, C. J., & Held, I. M. (2012). Detailed investigation of the self-aggregation of convection in cloud-resolving simulations. *Journal of the Atmospheric Sciences*, *69*(8), 2551–2565. https://doi.org/10.1175/JAS-D-11-0257.1

Muller, C. J., O'Gorman, P. A., & Back, L. E. (2011). Intensification of precipitation extremes with warming in a cloud-resolving model. *Journal of Climate*, *24*(11), 2784–2800. https://doi.org/10.1175/2011JCLI3876.1

Neelin, J. D., Peters, O., & Hales, K. (2009). The transition to strong convection. *Journal of the Atmospheric Sciences*, *66*(8), 2367–2384. https://doi.org/10.1175/2009JAS2962.1

Newton, C. W. (1966). Circulations in large sheared cumulonimbus. *Tellus*, *18*(4), 699–713. https://doi.org/10.1111/j.2153-3490.1966.tb00291.x

Nguyen, H., Protat, A., Kumar, V., Rauniyar, S., Whimpey, M., & Rikus, L. (2015). A regional forecast model evaluation of statistical rainfall properties using the CPOL radar observations in different precipitation regimes over Darwin, Australia. *Quarterly Journal of the Royal Meteorological Society*, *141*(691), 2337–2349.

O'Gorman, P. A. (2015). Precipitation extremes under climate change. *Current Climate Change Reports*, *1*(2), 49–59. https://doi.org/10.1007/s40641-015-0009-3

O'Gorman, P. A., & Schneider, T. (2009). The physical basis for increases in precipitation extremes in simulations of 21st-century climate change. *Proceedings of the National Academy of Sciences*, *106*(35), 14,773–14,777. https://doi.org/10.1073/pnas.0907610106

Oury, S., Dou, X., & Testud, J. (2000). Estimate of precipitation from the dual-beam airborne radars in TOGA COARE. Part II: Precipitation efficiency in the 9 February 1993 MCS. *Journal of Applied Meteorology*, *39*(12), 2371–2384. https://doi.org/10.1175/1520-0450(2000)039<2371:EOPFTD>2.0.CO;2

Pfahl, S., O'Gorman, P. A., & Fischer, E. M. (2017). Understanding the regional pattern of projected future changes in extreme precipitation. *Nature Climate Change*, *7*(6), 423–427. https://doi.org/10.1038/nclimate3287

Pope, M., Jakob, C., & Reeder, M. J. (2009). Regimes of the North Australian wet season. *Journal of Climate*, *22*(24), 6699–6715. https://doi.org/10.1175/2009JCLI3057.1

Protat, A., Rauniyar, S., Kumar, V. V., & Strapp, J. W. (2014). Optimizing the probability of flying in high ice water content conditions in the tropics using a regional-scale climatology of convective cell properties. *Journal of Applied Meteorology and Climatology*, *53*(11), 2438–2456. https://doi.org/10.1175/JAMC-D-14-0002.1

Protat, A., & Williams, C. R. (2011). The accuracy of radar estimates of ice terminal fall speed from vertically pointing Doppler radar measurements. *Journal of Applied Meteorology and Climatology*, *50*(10), 2120–2138. https://doi.org/10.1175/JAMC-D-10-05031.1

Seeley, J. T., & Romps, D. M. (2015). Why does tropical convective available potential energy (CAPE) increase with warming? *Geophysical Research Letters*, *42*, 10,429–10,437. https://doi.org/10.1002/2015GL066199

Singh, M. S., Kuang, Z., Maloney, E. D., Hannah, W. M., & Wolding, B. O. (2017). Increasing potential for intense tropical and subtropical thunderstorms under global warming. *Proceedings of the National Academy of Sciences*, *114*(44), 11,657–11,662. https://doi.org/10.1073/pnas.1707603114

Singh, M. S., & O'Gorman, P. A. (2013). Influence of entrainment on the thermal stratification in simulations of radiative-convective equilibrium. *Geophysical Research Letters*, *40*, 4398–4403. https://doi.org/10.1002/grl.50796

Singh, M. S., & O'Gorman, P. A. (2014). Influence of microphysics on the scaling of precipitation extremes with temperature. *Geophysical Research Letters*, *41*, 6037–6044. https://doi.org/10.1002/2014GL061222

Singh, M. S., & O'Gorman, P. A. (2015). Increases in moist-convective updraught velocities with warming in radiative-convective equilibrium. *Quarterly Journal of the Royal Meteorological Society*, *141*(692), 2828–2838. https://doi.org/10.1002/qj.2567

Steiner, M., Houze, R. A. Jr., & Yuter, S. E. (1995). Climatological characterization of three-dimensional storm structure from operational radar and rain gauge data. *Journal of Applied Meteorology*, *34*(9), 1978–2007.

Sui, C.-H., Li, X., & Yang, M.-J. (2007). On the definition of precipitation efficiency. *Journal of the Atmospheric Sciences*, *64*(12), 4506–4513. https://doi.org/10.1175/2007JAS2332.1

Tan, J., & Oreopoulos, L. (2019). Subgrid precipitation properties of mesoscale atmospheric systems represented by MODIS cloud regimes. *Journal of Climate*, *32*(6), 1797–1812. https://doi.org/10.1175/JCLI-D-18-0570.1

Thompson, E. J., Rutledge, S. A., Dolan, B., Thurai, M., & Chandrasekar, V. (2018). Dual-polarization radar rainfall estimation over tropical oceans. *Journal of Applied Meteorology and Climatology*, *57*(3), 755–775.

Williams, C. R. (2012). Vertical air motion retrieved from dual-frequency profiler observations. *Journal of Atmospheric and Oceanic Technology*, *29*(10), 1471–1480. https://doi.org/10.1175/JTECH-D-11-00176.1

Xie, S., Hume, T., Jakob, C., Klein, S. A., McCoy, R. B., & Zhang, M. (2010). Observed large-scale structures and diabatic heating and drying profiles during TWP-ICE. *Journal of Climate*, *23*(1), 57–79. https://doi.org/10.1175/2009JCLI3071.1

Zhang, M. H., & Lin, J. L. (1997). Constrained variational analysis of sounding data based on column-integrated budgets of mass, heat, moisture, and momentum: Approach and application to ARM measurements. *Journal of the Atmospheric Sciences*, *54*(11), 1503–1524. https://doi.org/10.1175/1520-0469(1997)054<1503:CVAOSD>2.0.CO;2